IOP Publishing Journal of Physics: Condensed Matter
J. Phys.: Condens. Matter **28** (2016) 015601 (9pp) doi:10.1088/0953-8984/28/1/015601

Core-resonant double photoemission from palladium films

I Kostanovskiy[1], F O Schumann[1], Y Aliaev[1], Z Wei[1] and J Kirschner[1,2]

[1] Max-Planck Institut für Mikrostrukturphysik, Weinberg 2, 06120 Halle, Germany
[2] Institut für Physik, Martin-Luther Universität, von-Danckelmann-Platz 3, 06120 Halle, Germany

E-mail: ikost@mpi-halle.de

Received 30 July 2015, revised 28 October 2015
Accepted for publication 12 November 2015
Published 9 December 2015

Abstract

We studied the core-resonant double photoemission process from palladium films with linearly polarized synchrotron radiation. We excited either the 3*d* or 4*p* core level and focused on the Auger transitions which leave two holes in the valence band. We find that the two-dimensional energy distributions are markedly different for the 3*d* and 4*p* decay. The 3*d* decay can be understood by a sequential emission of the two electrons while the 4*p* decay proceeds in a single step. Despite the large differences in the two-dimensional energy spectra we find the shape of the energy sum spectra rather similar. For the description of the 4*p* decay we propose a model which uses available single electron spectra, but suggest an alternative interpretation of these data. With this we are able to explain the range over which the available energy is shared. Key assumptions of the model are verified by our experiments on the 3*d* decay.

Keywords: photoemission, Auger, APECS

(Some figures may appear in colour only in the online journal)

I. Introduction

Auger electron spectroscopy is a powerful tool to characterize the chemical state of surfaces. It is based on the observation that each element emits electrons with specific kinetic energies once a core electron is removed. This is usually facilitated by the use of an electron gun or photon source which posses energies exceeding the binding energy of the core level.

Besides its practical importance for surface science Auger spectroscopy allows also to probe the electron correlation. Due to the fact that a core and an Auger electron has been emitted the sample has lost two electrons. From this point of view it is obvious that electron correlation plays a role. The rearrangement of the electrons may involve two valence electrons and the Auger spectra of these core-valence-valence (CVV) transitions provide access to the electron correlation energy within the valence band [1, 2].

In this context the energetic position and shape of the Auger spectrum of CVV transitions has been of interest. The simplest model proposed to describe the Auger spectrum is to use a self-convolution of the density-of-states (DOS) of width W [3]. This predicts an Auger spectrum of width $2W$. However, it was soon recognized that some materials could not be adequately described in this way. On the one hand the Auger spectra were narrower than $2W$, on the other hand the energetic position was shifted by a value U_{eff} from the value expected by the binding energy values of the participating electronic levels. This entity represents the effective electron-electron correlation energy. Experimentally a systematic behavior was identified [4]. For $U_{\mathrm{eff}} \ll W$ the line shape was well described by the self-convolution of the density of states (or band-like behavior) while for $U_{\mathrm{eff}} \gg W$ the spectrum becomes atomic like and the multiplet description applies. These findings could be captured by the Cini-Sawatzky (CS) theory which computes the Auger spectrum via a transformation of the DOS which includes the Coulomb correlation [1, 2]. The latter was described by the Hubbard parameter U. Pd films have been investigated as far as the CVV decay is concerned where the 3*d* core level was involved [5–7]. For this material $U/W \approx 0.8$ hence its Auger lineshape is in the intermediate region between a band-like and atomic like behavior. The complexity of the Auger spectra can be reduced by electron coincidence spectroscopy and significant experimental advances have been made in the past [6, 8–13].

A detailed coincidence investigation of Pd revealed that a straightforward application of the CS theory could not

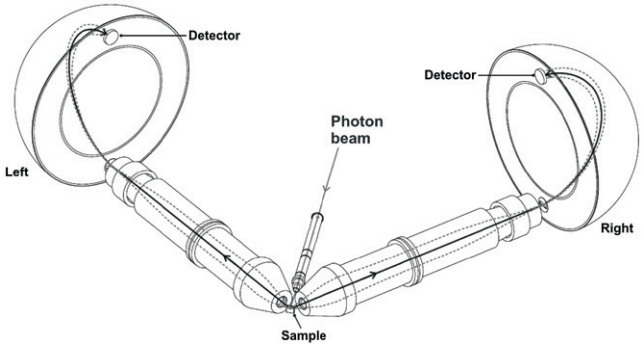

Figure 1. Overview of the coincidence setup. The key components are a pair of hemispherical analyzers, the axes of their transfer lenses define a scattering plane. Within this plane lies the photon beam and the linear polarization of the light. We used a beamline at the BESSY II storage ring described in more detail by Sawhney *et al* [18].

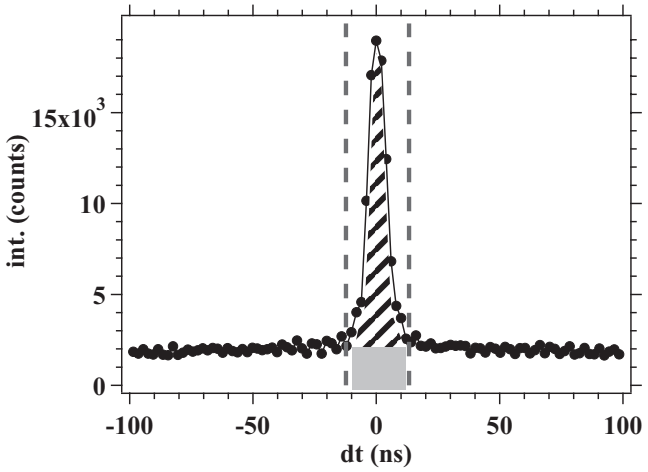

Figure 2. Typical arrival time histogram for a double photoemission (DPE) experiment on Pd. The emergence of a peak is evidence of 'true' coincidences while the constant intensity outside the peak region is due to 'random' coincidences. The vertical dashed lines mark the region which we used to compute energy distributions. The width of the peak is 10 ns.

reproduce the spectra. Instead one had to resort to an individual transformation of multiplet terms [7]. Our interest in Pd stems from the fact that it is included in a series of elements ranging from Mo to Xe which are characterized by an increasing 4*p* line width until the element Xe [14, 15].

In this work we discuss the CVV transition of Pd films using synchrotron radiation and a coincidence spectrometer. We excite either the 3*d* and 4*p* core level and observe a very different behavior of the 2D-Energy spectra while the energy sum spectra are rather similar. Like in our previous study on the 3*d* and 4*p* decay of Ag we find that the 3*d* decay can be explained by a sequential emission of the two electrons. The 4*p* decay proceeds in a way consistent with a single step process. In contrast to the extensive energy sharing seen in the 4*p* decay of Ag we see a narrower distribution. We can understand this observation by an alternative interpretation of single electron spectra. We explain the underlying model which uses as input parameter published spectroscopic data. An additional assumption is verified by our coincidence measurements on the Pd 3*d* decay, which agree with previous coincidence studies [6, 7].

II. Experiment

All experiments were done in a UHV μ-metal vacuum chamber with a base pressure of $2 \cdot 10^{-10}$ mbar. This instrument is equipped with standard surface science tools like LEED and Auger spectroscopy. The details of the coincidence apparatus are discussed in detail elsewhere [16, 17]. Here we recall the most important features.

Key components are a pair of hemispherical electron energy analyzers (VG Scienta R4000) with a mean radius of 200 mm. Electrons emitted from the surface are collected by the wide-angle electron lens with an angular range of $+/-15°$, see figure 1. After energy dispersion in the hemisphere the electrons are detected by a micro channel plate (MCP) with position sensitivity via a resistive anode. The energy window seen by each analyzer is about 9% of the pass energy. In order to have a sufficiently large energy range we performed our studies with a pass energy of 300 eV which yields a width of 27 eV. We routinely check this via the elastic peak of a electron gun measured at different primary energies. The energy resolution with 1 mm slits was better than 0.8 eV. In contrast to the usual way of recording spectra via scanning the kinetic energy we fix all lens voltages for a given photon energy. For all experiments we tuned both spectrometer to cover the same energy window. The energy scale of both analyzers was calibrated with the XPS and Auger peaks of silver and palladium.

We operate the coincidence circuit such that the arrival time difference of two electrons at the respective detectors is in a time interval of ± 100 ns, the time resolution of the electronics is about 1 ns. In figure 2 we present a typical arrival time histogram. The horizontal and vertical axes correspond to the time difference Δt and the number electron pairs in counts, respectively. The histogram is dominated by a peak centered at zero with a width of 10 ns which resides on a constant background. The peak is evidence of 'true' coincidences by which is meant that a single photon caused the emission of two electrons. The width of the peak is a reflection of the time resolution of the instrument which is largely given by the flight time differences in the hemispheres [19, 20]. The constant background stems from the excitation of two electrons via two uncorrelated photons and these contributions are called 'random' coincidences. For the generation of energy spectra we select only those events with Δt values within the region marked by the pair of dashed lines. The hatched intensity corresponds to the 'true' coincidences. The constant background under the peak, which is shown with a grey color, represents the contribution of the 'random' coincidences. The intensity of the 'true' coincidences is proportional to the intensity of the primary flux, while the intensity of the 'random' coincidences depends quadratically on the flux. Therefore, one has to significantly reduce the primary flux. We operate with a flux of the order of $2 \cdot 10^6$ photons/s as measured with a MCP brought into the sample position. We should emphasize that

this flux is several order less than the value for the standard photoelectron spectroscopy measurements.

Conceptionally it is not possible to separate the contribution of the 'random' events from those termed 'true'. However one can remove the aggregate effect by following standard procedures documented in the literature [21, 22]. We described the implementation of these for our instrument previously [17].

The studies were performed at the UE56/2-PGM-2 beamline of the BESSY II synchrotron storage ring (Berlin) [18]. The photon beam impinges at normal incidence onto the sample, while the analyzers are collecting electrons within an angle of $45 \pm 15°$. We selected linearly polarized light with the polarization within the scattering plane.

The Pd films were prepared by an e-beam evaporator EGC04 from Oxford Applied Research on a Ag(1 0 0) surface. This surface was cleaned in a standard manner by several cycles of Ar^+ ion sputtering and annealing at 450 °C. The quality of the resulting Ag surface was investigated via LEED which indicated a sharp diffraction pattern indicative of a well-ordered (1 0 0) surface. Via Auger electron spectroscopy (AES) we confirmed the cleanliness of the substrate and the Pd films. The evaporation process was divided in steps each of them followed by a AES measurement. After 20 min of total evaporation time we could not observe the intensity of the silver MVV Auger peak. We esimate the thickness to be about 3 nm.

III. Energy relations in the double photoemission process

In this section we want to describe simple energy relations between the emitted electrons in the double photoemission (DPE) process leading to Auger electron emission. We will demonstrate how standard XPS/Auger data can be interpreted to predict the 2D-Energy distribution of the emitted pair in such a DPE experiment. We want to discuss the implication for the specific case of DPE from Pd in which either a 3*d* or 4*p* photoelectron is emitted and the emission of the decay electron involves the 4d valence states. We will refer to these processes as 3*d* or 4*p* decay, respectively.

Suppose we detect two electrons in coincidence which posses kinetic energies E_1 and E_2, respectively. Inevitably the energy distribution of pairs is a two-dimensional entity. The natural choice is to use a coordinate system in which the individual energies represent the two orthogonal axes marked black in figure 3(a). Consequently a coincidence event has the coordinates (E_1, E_2). In this work we present the 2D-Energy distributions in this manner.

Nevertheless an electron pair can also be characterized by its energy sum $E_{\mathrm{sum}} = E_1 + E_2$ and energy sharing (difference) $E_{\mathrm{shar}} = E_1 - E_2$. In this case one has to use another coordinate system depicted by the red axes in figure 3(a) and the coincidence event has now the coordinates ($E_1 + E_2$, $E_1 - E_2$).

We quote the kinetic energy of the electrons with respect to the vacuum level of the sample. On this scale the kinetic energy of the Auger electron is independent of the photon energy, while the photo electron peak moves linearly with

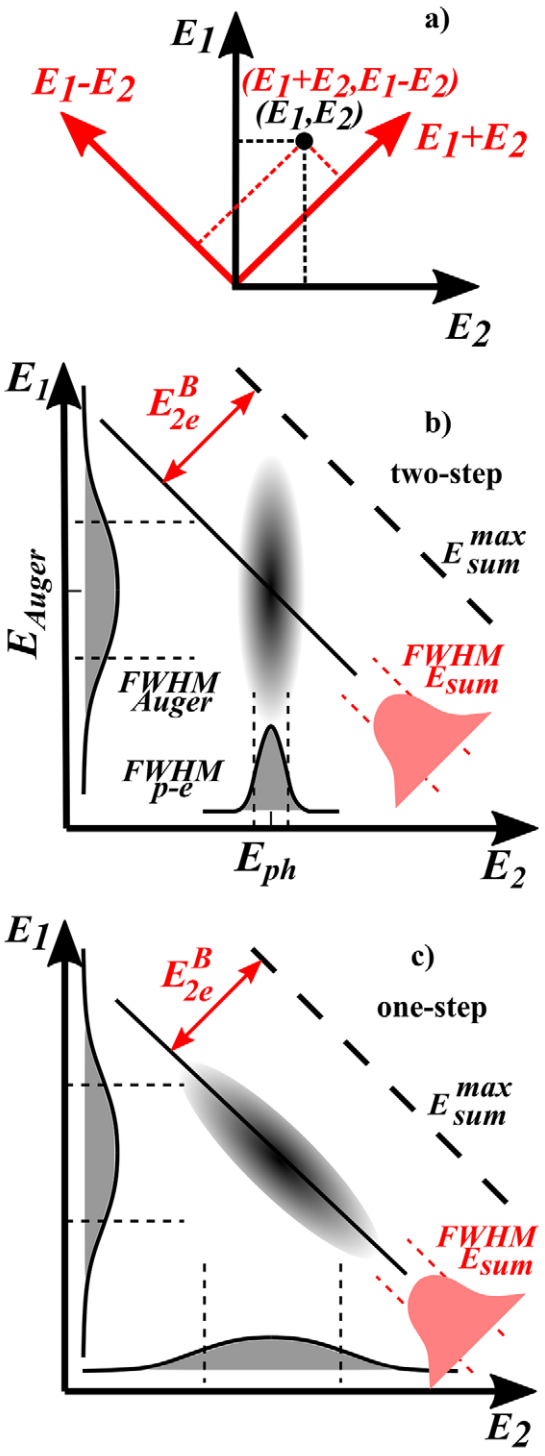

Figure 3. In (a) we present two different coordinate systems which can be used to specify the energy coordinates of an electron pair. Two possible outcomes of the 2D-Energy distribution of a DPE experiment [23]. In (b) we present the case where the emission of a photo and Auger electron is sequential (two-step). The spectrometer tuned to the photoelectron line will measure a narrow line with a width $\mathrm{FWHM_{ph}}$ while the other spectrometer covers an Auger line with larger width $\mathrm{FWHM_{Auger}}$. In (c) we present an outcome which was recently presented in the 4*p* decay of Ag [23]. Now the intensity is distributed along a diagonal direction.

photon energy. The energy sum of a pair has an upper bound given by $E_{\mathrm{sum}}^{\mathrm{max}} = h\nu - 2\phi$ which is the difference between the photon energy and twice the work function ϕ. This term describes the emission of two electrons from the Fermi level E_{F}. If we use $E_{\mathrm{sum}}^{\mathrm{max}}$ as a reference energy we can compute the difference $E_{\mathrm{sum}}^{\mathrm{max}} - E_{\mathrm{sum}}$. In doing so we have derived the two-electron binding energy E_{2e}^{B}. In such a presentation the spectral feature of the sum energy will not change its energy position upon the variation of the photon energy as we are accustomed to in single photoelectron emission.

For the 4d transition metals the 3*d* photoelectron line and associated Auger electron have well defined energy positions and width. Therefore we can expect that the 2D-Energy distribution of a coincidence experiment may have the form depicted in figure 3(b). In this picture one assumes that the emission of the electrons occurs sequentially (two-step process). For simplicity we imagine that the photon energy has been selected to ensure that there is no spectral overlap between Auger and photo electron. Additionally we ignore spin–orbit split photoelectrons. The photoelectron is detected via a spectrometer whose energy axis is along the *x*-axis while the broader Auger line is covered by another spectrometer with the energy axis along the *y*-axis. We simulate this 2D-Energy distribution for simplicity by a 2D-Gaussian function $G(E_1, E_2)$ which is the product of two Gaussians. One term depends on the energy E_1 while the other depends on E_2, hence we write $G(E_1, E_2) = G_1(E_1) \cdot G_2(E_2)$. The coordinates of the maximum intensity are determined by the central energies of the Auger and photoelectron lines. The projection of this 2D Gaussian onto the two axes gives the width of the lines as evidenced by single electron spectroscopy. The larger width of the Auger line is due to the fact that two electrons from the 4d valence level are involved.

We have added to the schematic in figure 3(b) two important diagonal lines. The dashed line labels the $E_{\mathrm{sum}}^{\mathrm{max}}$ position while the solid line marks the sum energy given by the peak positions of the Auger and photoelectron line. The energetic separation between these two lines is the aforementioned two-particle binding energy E_{2e}^{B}. The simulated 2D-Energy distribution can also be projected onto the E_{sum} or $E_1 + E_2$ direction which yields a spectrum sketched in red. Its width is mainly given by the width of the Auger line, but the photoelectron width can not be ignored.

In our previous work on the 4*p* decay of Ag we have demonstrated that another shape of the 2D-Energy map is possible which we schematically present in figure 3(c) [23]. Rather than an intensity distribution which is aligned along the *y*-axis we notice an intensity feature which is parallel to the solid diagonal line. This means the decay is characterized by a well-defined sum energy value of the pairs. Its width can be assessed by the red spectrum in figure 3(c). Such an emission of electron pairs has to be an one-step process. The dashed diagonal line, represents the two particle binding energy E_{2e}^{B} as in figure 3(b). If only one spectrometer is available the diagonal intensity distribution will show up as a broad feature as indicated by the projection onto the E_1 and E_2 axes. The intensity distribution of figure 3(c) has also been modelled by a 2D-Gaussian, which again is a product of two Gaussians. However, this time we write $G(E_1, E_2) = G_1(E_1 + E_2) \cdot G_2(E_1 - E_2)$. This means we use the energy sum and sharing of a pair as coordinates, conversely we use the coordinate system with the red axes in figure 3(a). In this context we recall a well-known observation that for the materials starting from Mo in the periodic table one notices a systematic increase of the 4*p* line width until the element Xe is reached [14, 15]. This unusual feature was explained by a rapid fluctuation between two different configurations [15]. As a consequence of energy conservation this should result in a diagonal intensity feature as shown in figure 3(c). This was exactly our experimental observation in the case of the 4*p* decay of Ag [23].

Table 1. The input parameters for our model originate from standard sources of XPS spectra.

	Pd	Ag	In
Work function	5.65	4.64	4.1
E_{2e}^{B}	8.4	17.4	41.3
E_{4p}^{B}	52	60	78
FWHM_{3d}	1.1	0.29	0.98
FWHM_{4p}	5.8	14	26
FWHM_{3dVV}	5.5	2.7	2.8

Note: All values are given in eV [24, 25].

This motivates us to try to predict the outcome of an experiment studying the 4*p* decay. For this we want to use as input the width and energy position of the 3*d* photoelectron and the related CVV Auger electron. Furthermore, we assume that the observed large width of the 4*p* photoelectron is a consequence of a broad diagonal intensity feature in the 2D-energy spectra. Finally we assume that the two-particle binding energy of the 3*d* and 4*p* decay is the same as experimentally determined in our work on the 4*p* decay of Ag [23]. Upon a suitable choice of the photon energy the kinetic energy of the 4*p* electron is well outside the secondary electron region. However, this is not true for the Auger electron. In the case of Pd the 4*p* level has a binding energy 52.4 eV. This limits the kinetic energy for the Auger electron in this decay and it will fall into the secondary electron region. Therefore the Auger electron related to the 4*p* decay of the materials ranging from Pd to Xe are not identified in single electron spectroscopy. Only in the derivative spectra peaks exist [26], but the important assessment about the width is not possible in these spectra. Our aim is to circumvent this by a new interpretation of available single electron spectra. First, we assume that the 4*p* decay proceeds in a way as sketched as in figure 3(c). Second, we assume that the width of the sum energy spectrum (indicated by the red spectrum) has the same width and binding energy E_{2e}^{B} as in the 3*d* decay. Third, the observed width of the 4*p* photoelectron is due to the projection of a diagonal intensity feature. In this case the kinetic energy of the 4*p* Auger electron is uniquely defined. The material dependent parameters we used for the modeling of the 4*p* decay of Ag and Pd are listed in table 1. These we have taken from available standard XPS data,

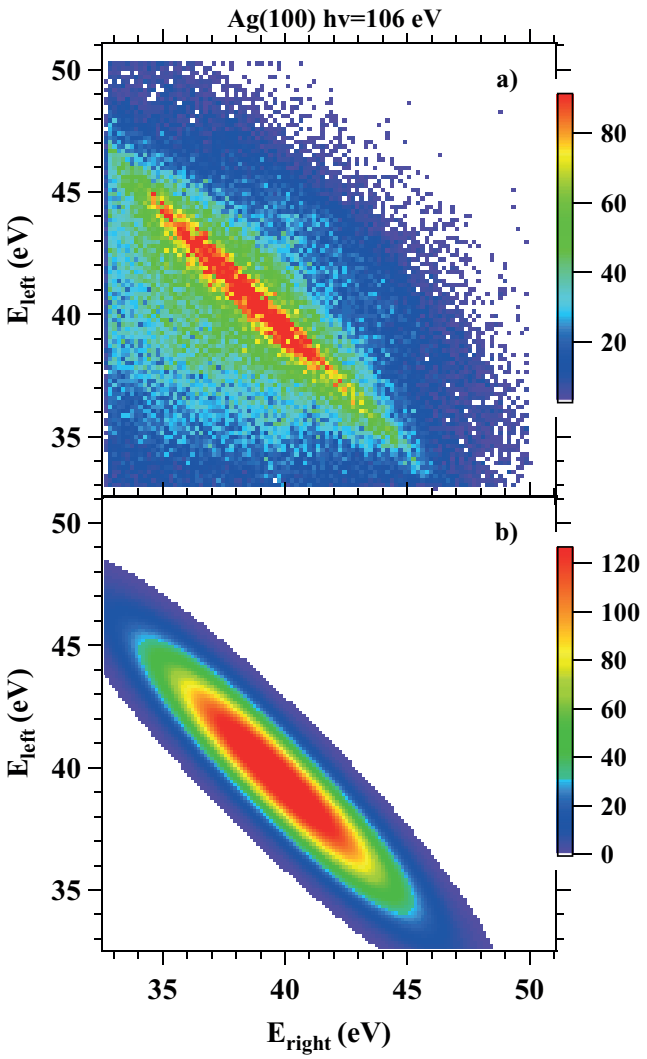

Figure 4. In panel (a) we show the experimental energy distribution from an experiment on a Ag (1 0 0) surface. The photon energy is 106 eV. In panel (b) we present the result from our model as explained in the text.

we emphasize that there are no adjustable parameters within our model [24, 25].

In figure 4(a) we present the 2D-Energy distribution obtained from an experiment studying the 4*p* decay of Ag with a photon energy of 106 eV and contrast it with our model. Clearly the alternative interpretation of the spectroscopic data is justified by the good agreement with the data. We point out that our model does not include intensity due to the direct DPE process in which two valence electron are emitted without participation of a core level.

In previous DPE experiments on Ni and Cu samples with a photon energy of 45 eV we can not excite any core levels. Therefore, any observable intensity comes from a direct DPE process involving the valence states [27–29]. In first approximation the intensity maximum of the direct DPE can be determined by the self-convolution of density of states. This leads for the case of Pd to a peak at $E_{2e}^{\mathrm{B}} = 3.5$ eV. In the discussion of the energy sum spectra it will be apparent that in the photon energy range used in this work there is no peak at this position. Therefore, we can ignore the contribution of direct DPE.

IV. Results

IV.A. Pd 4p decay

Having introduced the model and checking its usefulness in the Ag 4*p* decay we proceed in presenting the data of our Pd 4*p* experiments together with result of the model using the parameters of table 1. In figure 5 we present them for a photon energy of 100 eV. In the experimental plot figure 5(a) we have removed the intensity in the lower left corner in order to emphasize less intense energy features in the region of interest. The dashed diagonal line indicates the position of $E_{\mathrm{sum}}^{\mathrm{max}}$ while the solid diagonal line marks the nominal position of the sum energy on the basis of our model. This means we expect the intensity of the 4*p* decay to be in the vicinity of this line. We see that upon approaching the $E_{\mathrm{sum}}^{\mathrm{max}}$ line the intensity drops. Any intensity above the line is due to random coincidences. We notice an intensity maximum near the solid line if the outgoing Auger and photoelectron have the same energy of about 40 eV. If we compare this with the outcome of our model for the one-step decay in figure 5(b), we have a good agreement. We do not observe an extended diagonal intensity band like for the 4*p* decay of Ag, see figure 4. This is an immediate consequence of the smaller 4*p* photoelectron line width of Pd compared to Ag, see table 1.

It is appealing to generate a 2D-Energy spectrum assuming a two-step decay. The result is presented in figure 5(c) and it is obvious that this spectrum does not resemble our data. Additionally it is worth mentioning that in figure 5(c) the line width of the Auger spectrum is significantly smaller than the photoelectron line width. The white arrow indicates this width for the Auger electron projected onto the *y*-axis, while the black arrow shows the width of the photoelectron projected onto the *x*-axis. This is an unphysical result, because in the two-step picture the photoelectron is emitted first and then two valence states are involved in the Auger electron emission. The valence band has a finite width, hence the Auger electron width can not be smaller than the photoelectron width.

We are forced to assume a narrow Auger line, because of the constraint on the width of the E_{sum} spectrum in the 4*p* decay. According to our description it is given by the width of the Auger and photoelectron line of the 3*d* decay. We will provide the proof of this assumption in the context of our discussion of the 3*d* decay in the next section. In principle it could have been possible that the 4*p* decay proceeds in a one-step and two-step fashion. By this it is meant that the experiment measures a statistical average of the two decay paths. This we can rule out, because of the unphysical result for the Auger line width for the two-step decay.

In figure 6 we present the 2D-Energy distributions for a photon energy of 110 eV. The experimental spectrum in (a) shows two intensity maxima near the solid diagonal line which marks the predicted position of the E_{sum} value for the 4*p* decay. Due to the increase of the photon energy by 10 eV the photoelectron has now a kinetic energy of about 50 eV, while the energy of the Auger electron is still at the value of around 40 eV, as in figure 5(a). The simulated spectrum obtained from our model for a one-step decay resembles

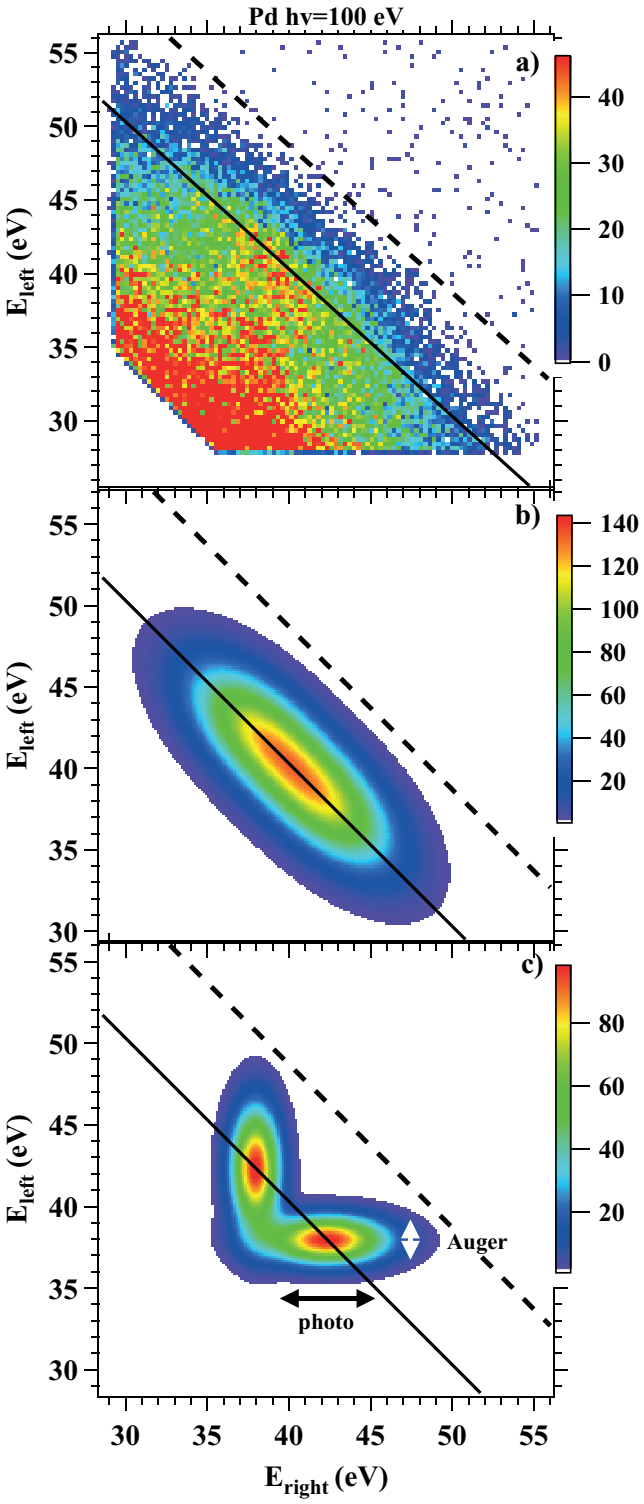

Figure 5. In (a) we present the experimental DPE intensity from the Pd film for $h\nu = 100$ eV. The dashed diagonal line represents $E_{\mathrm{sum}}^{\mathrm{max}}$. The solid line marks the energy position were we expect the intensity due to the 4*p* decay. In (b) we present the outcome of our model for an one-step decay. In (c) we present the energy distribution for a two-step decay. To the intensity pocket at the lower right-hand corner we have added two arrows indicating the projected width of the Auger and photoelectron.

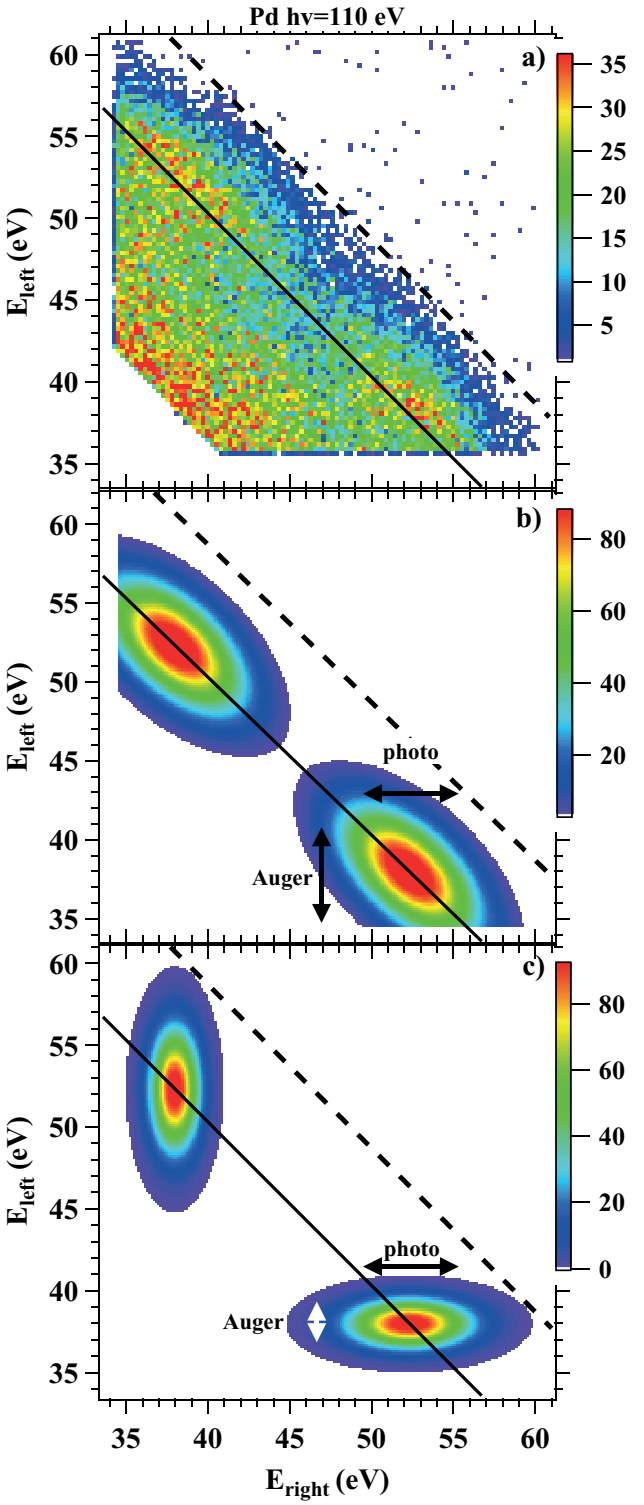

Figure 6. In (a) we present the experimental DPE intensity from the Pd for $h\nu = 110$ eV. The dashed diagonal line represents $E_{\mathrm{sum}}^{\mathrm{max}}$. The solid line marks the energy position were we expect the intensity due to the 4*p* decay. In (b) we present the outcome of our model if we assume a one-step decay. In (c) we present the energy distribution if assume a two-step decay. The arrows in (b) and (c) indicate the width of the projection of the Auger and photoelectron onto the respective axis.

the observation rather well, see figure 6(b). This is in contrast to a two-step type decay presented in figure 6(c) which clearly is at odds with the measured spectrum. In analogy to the spectrum in figure 5(c) the Auger line width is much smaller than those of the 4*p* photoelectron. Again this is an unphysical result.

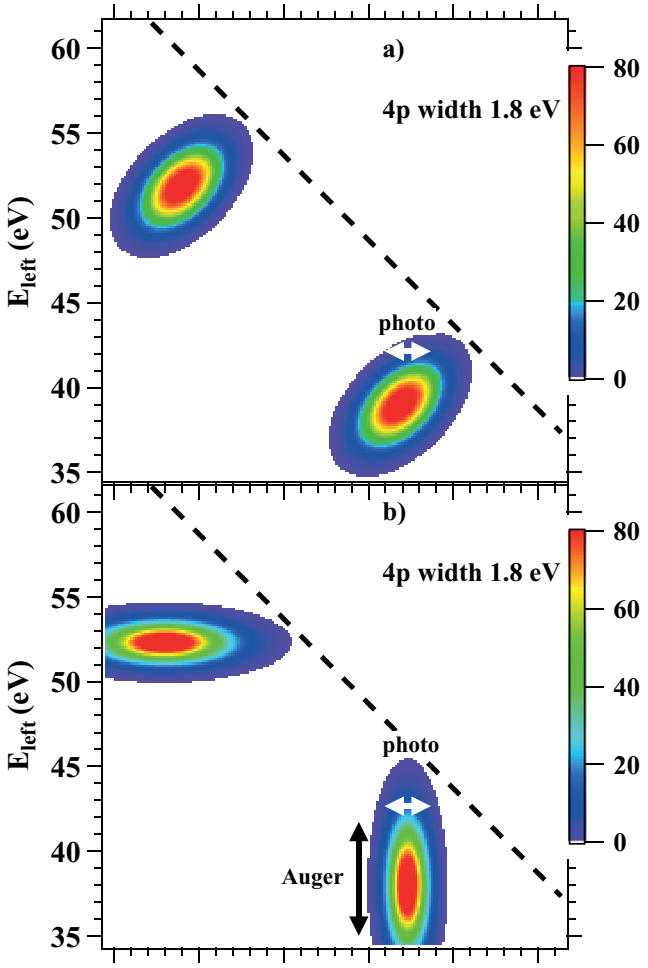

Figure 7. We present the hypothetical 2D-Energy distribution for Pd if the 4*p* line width is 1.8 eV. All other parameters are kept as shown in table 1. The dashed line indicates the $E_{\mathrm{sum}}^{\mathrm{max}}$ line. In (a) we plot the result for a one-step process, while in (b) the result for the two-step process is shown.

This means that spectroscopic data known from data bases are sufficient to predict the outcome of a DPE experiment. This is in particular interesting as far as the 4*p* decay is concerned for materials known to have a broad 4*p* photoelectron line. Among these materials is also In and we have added the relevant spectroscopic data in the table. We note that the 4*p* width is almost a factor 2 larger than the value for Ag. From this alone one may speculate that a DPE experiment on the 4*p* decay of In will show up as a diagonal intensity region which is even larger than those for Ag.

It is illustrative to discuss the potential outcome if we change some model parameters for Pd. We want to keep the parameter for the 3*d* decay unchanged. Therefore the two-particle binding energy is still at the value given in table 1. Consequently, the width of the sum energy spectrum for the 3*d* decay stays at the same value of 6 eV. This is the value we want to use for the prediction of the 4*p* decay. While keeping this width the same for the 4*p* decay, we want to change the 4*p* line width from 5.8 to 1.8 eV. This means the width of the 4*p* line is smaller than those of the E_{sum} spectrum. In figure 7(a) we display the model energy spectrum for an one-step decay. We notice that the 2D-Gaussian has the larger extension perpendicular to the $E_{\mathrm{sum}}^{\mathrm{max}}$ line. This is different from figure 6(b) where the 2D-Gaussian has its larger extension parallel to the $E_{\mathrm{sum}}^{\mathrm{max}}$. Although we set the 4*p* width to 1.8 eV (marked by the white arrow) it is obvious that in figure 7(a) the projection onto the *x*-axis is larger than this value. This means one can not achieve consistency if the 4*p* width is smaller than the E_{sum} width within a one-step picture. For this set of parameters only the two-step process is conceivable and the resulting model prediction is presented in figure 7(b).

It turns out that the relation of the 4*p* line width to the E_{sum} width of the 3*d* decay has some predictive power. If the the 4*p* line is about the width (or larger) than the E_{sum} spectrum than an one-step process is likely. If on the other hand a the 4*p* line is narrower than the E_{sum} spectrum a two-step decay is likely. The ultimate proof can only be obtained by coincidence spectroscopy.

IV.B. Pd 3d decay

Key input parameters for our model were the data from the 3*d* photoelectron and associated Auger decay. It was assumed that the 2D-Energy distribution resembles the one depicted in figure 3(b) representative for a sequential emission. Our experimental results on the Pd 3*d* Auger decay, shown in figure 8, verify this notion. We performed two sets of experiments with slightly different photon energies of 656.5 and 679.5 eV, respectively. This ensures that the Auger and photoelectron have similar kinetic energies. Therefore both lines are captured within the energy window of a single spectrometer. In both panels we have added two diagonal lines. The dashed diagonal line represents the maximum sum energy $E_{\mathrm{sum}}^{\mathrm{max}}$ while the solid line marks the peak position of the E_{sum} spectrum using the model parameter in table 1. The spin–orbit splitting of the 3*d* level amounts to 5.3 eV. Therefore we observe a pair of photoelectron lines labelled as $3d_{3/2}$ and $3d_{5/2}$. The red arrows facilitate the identification of their kinetic energy on the *x*-axis in figure 8(a). The actual values are 310.5 eV and 315.8 eV. The associated Auger lines, commonly termed M_5VV and M_4VV, have kinetic energies of 321.5 eV and 326.8 eV which can be read off the *y*-axis by red arrows. This means that the Auger electrons posses a higher kinetic energy than the photoelectrons. This order is reversed if the photon energy is increased to $h\nu = 679.5$ eV. Now the 3*d* lines are at 333.5 eV and 338.3 eV, see the red arrows in figure 8(b). The Auger electrons maintain the kinetic energy of 321.5 eV and 326.8 eV. In figure 8(a) we marked a region by a circle. Within this we notice 4 intensity peaks, the most prominent is at coordinates (315.8 eV, 315.8 eV). At first glance one would identify this with the detection of two $3d_{5/2}$ photoelectrons. This is energetically not possible with a single photon. The intensity peak arises from a coincidence of a photoelectron line with the loss tail of the Auger line. When they intercept both particles have the same energy. At this point one can not distinguish between Auger and photoelectrons. Likewise we can explain the other intensity pockets within the circle. Similarly the circle in figure 8(b) marks a region where the nominal energy coordinates indicate two Auger electrons.

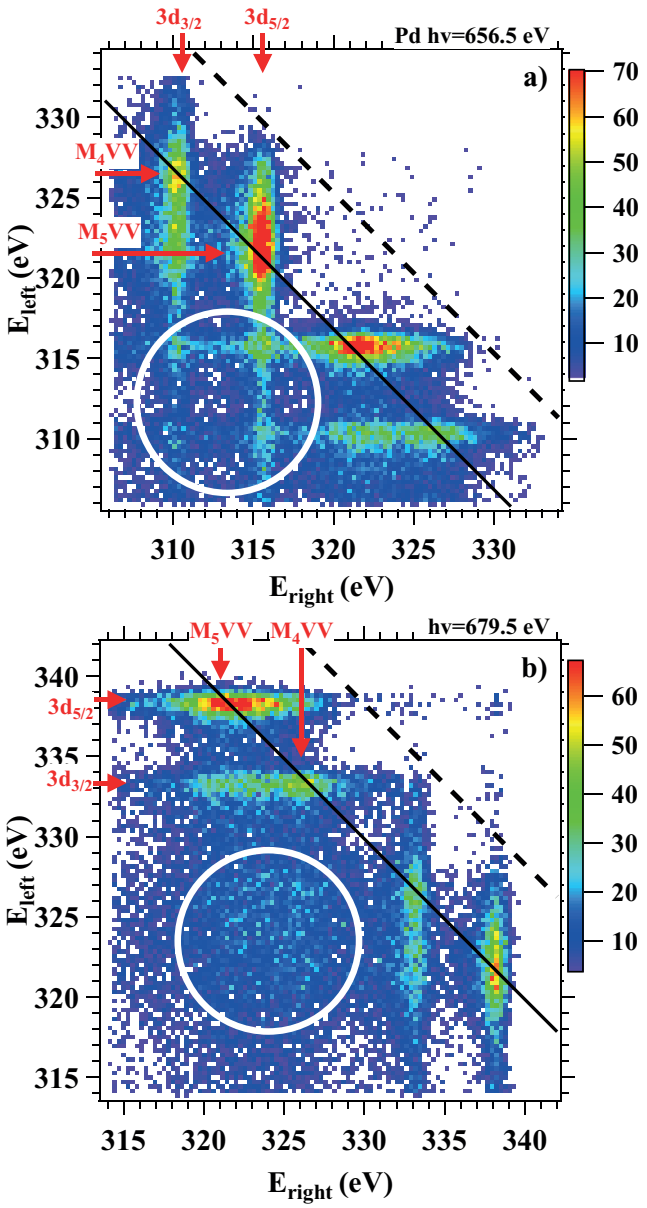

Figure 8. In (a) and (b) we plot the 2D-Energy distribution from a Pd film measured with the coincidence circuit with photon energy 656.5 eV and 679.5 eV, respectively. The dashed line represents the $E_{\text{sum}}^{\text{max}}$, while the solid line is defined by the E_{2e}^{B}. The white circles indicate the region where energy loss effects are observable.

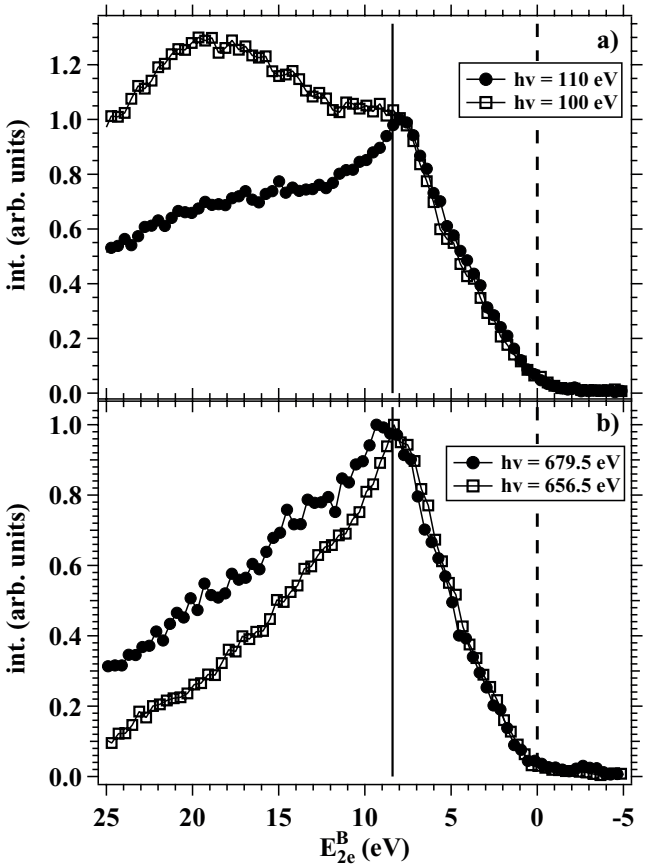

Figure 9. The sum energy spectra of the Pd 4*p*(a) and 3*d*(b) Auger decay as measured with different photon energies. $E_{\text{sum}}^{\text{max}}$ represented with the dashed line is a reference, while the solid line defined the E_{2e}^{B} value used in the model.

However, here we observe a photoelectron which experiences energy loss in coincidence with an Auger electron.

Moreover, in the experimental data for the 3*d* decay no diagonal-like energy features corresponding to an one-step decay are present. Therefore, we can prove that the 3*d* decay proceeds exclusively in a two-step fashion. The projection of the line structures onto the *x*- and *y*-axes yields spectra with sharp photoelectron and broad Auger peaks in a good agreement with the reference single electron XPS spectra. The analysis of the Auger line shape for a fixed energy of the photoelectron is also in a good agreement with the available APECS results [6, 7].

In both panels of figure 8 we can see that the solid line, representing the predicted peak of the E_{sum} spectrum, goes through the high intensity regions. In our model we assumed that the two-particle binding energy of the Auger-photoelectron pair remains constant for both the 3*d* and 4*p* Auger decay, which are characterized by the same final state. In order to prove this point we compare the E_{sum} spectra for the two decays. As energy scale we use the two-particle binding energy $E_{2e}^{\text{B}} = E_{\text{sum}}^{\text{max}} - E_{\text{sum}}$ introduced earlier. In figure 9 we present these spectra for the 4*p* (a) and 3*d* decay (b), respectively. These spectra were calculated by using the complete data sets, this means the omitted region in figures 5 and 6 are included in the E_{sum} data. For easier comparison of the spectra they are scaled such that they line up in the E_{2e}^{B} range 0–8 eV. The dashed vertical line in both panels marks the position of $E_{\text{sum}}^{\text{max}}$ which serves as energy reference set to zero. This is analogous to the usual practice in single electron spectroscopy. The vertical solid line corresponds to the calculated value of $E_{2e}^{\text{B}} = 8.4$ eV, see table 1. All spectra display a maximum near this energy except for the 4*p* experiment with 100 eV photon energy, see the open symbols in figure 9(a). For the latter we notice a shoulder near the solid line. Common to all spectra is a linear decrease of intensity towards $E_{2e}^{\text{B}} = 0$. For energies below $E_{2e}^{\text{B}} = 8.4$ eV there are differences between the results for the 4*p* and 3*d* decay. While for the 3*d* decay the intensity drops for larger E_{2e}^{B} values and adopts a triangular line shape

the 4*p* decay does have a higher intensity. This is even more pronounced for the 100 eV experiment where the intensity increases first. Inspection of figure 5 shows that the lowest detected energy is 30 eV which means that we are in a region into which the secondary electron tail extends. This contribution obviously affects the observed E_{sum} intensity. The slight differences between the E_{sum} spectra for the 3*d* decay below $E_{2e}^{\mathrm{B}} = 8.4$ eV are associated by the differences in the regions marked by the white circles in figure 8.

For our model several assumptions were made, which we proved in the experiment. The first assumption concerns two-particle binding energy which is the same for the 3*d* and 4*p* decay as evidenced by the sum energy peaks at 8.4 eV, see figure 9. The second point relates to the width the sum energy spectra. As it is evident from figure 9 both decays display a linear decrease of the intensity for energies above the peak position. For both studies the half width at half maximum is 3.5 eV . If we assume that the peak in the sum energy spectrum has a symmetric form, as within our model, than the full width is 7 eV. This is in reasonable agreement with the width we obtain simply by adding the photoelectron and Auger width which yields 6.6 eV according to table 1.

V. Conclusions

We have reported our results on the core-resonant double photoemission process of Pd films upon excitation of either the 3*d* and 4*p* levels. We have introduced a model aimed to predict the outcome of such experiments which has as the only input the electron spectroscopic data from data bases. The key point is an alternative interpretation of the single electron spectra. Applied to the case of the 4*p* decay of Pd we note good agreement if the decay proceeds via a one-step path. Compared to the Ag case the energy sharing is less pronounced for Pd. This is an immediate consequence of the smaller 4*p* photoelectron width of Pd compared to Ag. The investigation of the 3*d* decay of Pd further confirms a key assumption of the model. We find that the sum energy spectra for the 4*p* and 3*d* decay have essentially the same peak position and width/shape.

Acknowledgment

We would like to thank the staff of BESSY storage ring in particular B Zada and W Mahler for their excellent support. Funding from the DFG through SFB 762 is gratefully acknowledged.

References

[1] Sawatzky G A 1997 *Phys. Rev. Lett.* **39** 504
[2] Cini M 1977 *Solid State Commun.* **24** 681
[3] Lander J J 1953 *Phys. Rev.* **91** 1382
[4] Antonides E, Janse E C and Sawatzky G A 1977 *Phys. Rev.* B **15** 1669
[5] Weightman P, Wright H, Waddington S D, van der Marel D, Sawatzky G A, Diakun G P and Norman D 1987 *Phys. Rev.* B **36** 9098
[6] Creagh C A and Thurgate S M 2001 *J. Electron Spectrosc. Relat. Phenom.* **114116** 69
[7] Butterfield M T, Bartynski R A and Hulbert S L 2002 *Phys. Rev.* B **66** 115115
[8] Haak H W, Sawatzky G A and Thomas T D 1978 *Phys. Rev. Lett.* **41** 1825
[9] Jensen E, Bartynski R A, Hulbert S L, Johnson E D and Garrett R 1989 *Phys. Rev. Lett.* **62** 71
[10] Kakiuchi T, Kobayashi E, Okada N, Oyamada K, Okusawa M, Okudaira K K and Mase K 2007 *J. Electron Spectrosc. Relat. Phenom.* **161** 164
[11] Gotter R, Da Pieve F, Ruocco A, Offi F, Stefani G and Bartynski R A 2005 *Phys. Rev.* B **72** 235409
[12] Gotter R, Fratesi G, Bartynski R A, Da Pieve F, Offi F, Ruocco A, Ugenti S, Trioni M I, Brivio G P and Stefani G 2012 *Phys. Rev. Lett.* **109** 126401
[13] Filippo G D, Trioni M I, Fratesi G, Schumann F O, Wei Z, Li C H, Behnke L, Patil S, Kirschner J and Stefani G 2015 *J. Phys.: Condens. Matter* **27** 085003
[14] Kowalczyk S P, Ley L, Martin R L, McFeely F R and Shirley D A 1975 *Faraday Discuss. Chem. Soc.* **60** 7
[15] Wendin G 1981 *Breakdown of the One Electron Pictures in Photoelectron Spectra* (Berlin: Springer)
[16] van Riessen G A, Wei Z, Dhaka R S, Winkler C, Schumann F O and Kirschner J 2010 *J. Phys.: Condens. Matter* **22** 092201
[17] Schumann F O, Dhaka R S, van Riessen G A, Wei Z and Kirschner J 2011 *Phys. Rev.* B **84** 125106
[18] Sawhney K J S, Senf F, Scheer M, Schäfers F, Bahrdt J, Gaupp A and Gudat W 1997 *Nucl. Instrum. Methods* A **390** 395
[19] Völkel M and Sandner W 1983 *J. Phys.* E **16** 456
[20] Kugeler O, Marburger S and Hergenhahn U 2003 *Rev. Sci. Instrum.* **74** 3955
[21] Sawatzky G A 1988 Auger photoelectron coincidence spectroscopy *Auger Electron Spectroscopy* ed R P Messmer and C L Briant (New York: Academic)
[22] Jensen E, Bartynski R A, Hulbert S L and Johnson E 1992 *Rev. Sci. Instrum.* **63** 3013
[23] Wei Z, Schumann F O, Li C H, Behnke L, Di Filippo G, Stefani G and Kirschner J 2014 *Phys. Rev. Lett.* **113** 267603
[24] Moulder J F, Stickle W F, Sobol P E and Bomben K D 1992 *Handbook of X-ray Photoelectron Spectroscopy* (Eden Prairie, MN: Physical Electronics Division, Perkin-Elmer Corporation)
[25] NIST X-ray Photoelectron Spectroscopy Database, Version 4.1 2012 National Institute of Standards and Technology, Gaithersburg (http://srdata.nist.gov/xps)
[26] Childs K D, Carlson B A, LaVenier L A, Moulder J F, Paul D F, Stickle W F and Watson D G 1995 *Handbook of Auger Electron Spectroscopy* (Eden Prairie, MN: Physical Electronics Industries)
[27] Herrmann R, Samarin S, Schwabe H and Kirschner J 1998 *Phys. Rev. Lett.* **81** 2148
[28] Schumann F O, Winkler C and Kirschner J 2007 *Phys. Rev. Lett.* **98** 257604
[29] Schumann F O, Winkler C and Kirschner J 2009 *Physica Status Solidi b* **246** 1483